DOI: 10.1002/ejic.201100073

Site-Selective Chemical Reaction on Flexible Polymer Films for Tin Oxide Nanosheet Patterning

Yoshitake Masuda,*[a] Tatsuki Ohji,[a] and Kazumi Kato[a]

Keywords: Nanostructures / Tin oxide / Metal oxides / Polymers / Patterning / Site-selective deposition

Site-selective tin oxide deposition from aqueous solution was performed on super-hydrophilic surfaces. The chemical reaction and nucleation accelerated on hydroxy groups to form tin oxide nanosheets. Consequently, two-dimensional patterns of tin oxide nanosheets were fabricated on poly(ethylene terephthalate) (PET) films coated with indium tin oxide (ITO). Tin oxide sheets grew to 100–300 nm in-plane size and 5–10 nm thickness. Hydrophobic areas of the films suppressed formation of tin oxide structures. The site-selective chemical reaction can be applied to allow precise control of chemical reactions, surface coating, and two-dimensional patterning of tin oxide nanostructures for future devices.

Introduction

Tin oxide has been widely used, for instance in gas sensors,[1] optical devices,[2] lithium batteries,[3] biosensors,[4] and catalysts for chemical reactions (e.g., to convert anisole to 2,6-xylenol).[5] Various kinds of tin oxide nanostructures such as nanofibers,[6] nanowires,[7,8] nanobelts,[9] nanotubes,[10] nanorods,[11,12] spirals, nanorings,[13] zigzag nanobelts,[14] grains,[15] flakes,[15] plates,[15] meshes,[16] and columnar thin films[17] have been reported. Surface coating of substrates with tin oxide nanostructures are urgently required for future devices. In particular, 2D patterns of tin oxide nanostructures on flexible polymer films are required for light-weight, flexible sensors and solar cells. 2D patterning of nanomaterials[18,19] such as metal oxides,[20–25] Au clusters,[26] Pt nanoparticles,[27] organic monolayers,[28] bimolecular layers,[29] and DNA[30] is expected to lead to a large step forward in materials science research and the development of new devices.

Recently, syntheses of tin oxide nanostructures in aqueous solutions, enabling precise control of crystal growth, were developed. In addition, 2D patterning of metal oxides including amorphous tin oxide films[20] was realized with the use of self-assembled monolayers (SAMs).[21–25] Molecular recognition, organic–inorganic interactions, surface nucleation energy control, static interaction between SAMs and nanoparticles, and so on were effectively utilized for site-selective deposition of metal oxides. More recently, super-hydrophilic surfaces were used for 2D patterning of TiO_2 crystals.[31] F-doped SnO_2 transparent conductive film (FTO) substrates were modified to have super-hydrophilic/hydrophobic patterns. TiO_2 nanocrystals were formed in a site-selective manner on the super-hydrophilic areas of the substrates to create 2D patterns of TiO_2 without the use of self-assembled monolayers.

Light irradiation has been used for surface modification and material synthesis. Light irradiation was, for instance, used to clean TiO_2 surfaces and to connect oxide nanoparticles without heat treatment. TiO_2 nanocrystals were irradiated with UV light for 3 h to yield porous TiO_2 electrodes.[32] A medium pressure Hg lamp was used to prepare porous TiO_2 films for dye-sensitized solar cells.[33] UV/O_3 treatment of the indium tin oxide / poly(ethylene terephthalate) (ITO/PET) films before TiO_2 paste application slightly improved the cell efficiency of the dye-sensitized solar cell.[34] Light irradiation was effective in controlling nucleation and growth of crystals.[35–42] Self-assembled monolayers having octadecyl or amino head groups were modified to silanol groups with the irradiation. In aqueous solutions, metal oxides formed on silanol groups in a site-selective manner to yield nano/micropatterns of metal oxides. Light irradiation has been an effective strategy for the formation of nanostructures and for applications in devices. It has the advantage of being a simple, low-cost, and ordinary-temperature process, suitable for surface treatment of polymer films with low heat resistance.

Here we report a process to realize micropatterning of tin oxide nanosheets on flexible polymer films. In this study, flexible polymer films were exposed to light through a photomask to provide super-hydrophilic/hydrophobic patterns. In aqueous solutions, tin oxide nanosheets were crystallized on the super-hydrophilic areas in a site-selective manner to achieve 2D patterning of tin oxide nanosheets on flexible polymer films.

[a] National Institute of Advanced Industrial Science and Technology (AIST),
2266-98 Anagahora, Shimoshidami, Moriyama-ku, Nagoya 463-8560, Japan
E-mail: masuda-y@aist.go.jp

Supporting information for this article is available on the WWW under http://dx.doi.org/10.1002/ejic.201100073.

Results and Discussion

Surface Modification of ITO/PET Films and Deposition of Tin Oxide

The flexible poly(ethylene terephthalate) (PET) films coated with indium tin oxide (ITO) initially had a hydrophobic surface with a water contact angle of 111°. The design of photomask shown in Figure 1 dictated the size and shape of the pattern of the VUV-irradiated surfaces. After irradiation, these surfaces were wetted completely (contact angle 0–5°). In addition, the hydrophilic surface of ITO was much more densely covered with hydroxy groups than the hydrophobic surface of ITO before the irradiation. The initial surfaces of ITO and pure In_2O_3 crystals were covered with adsorbed organic molecules, which increased the water contact angle. The surface hydroxy groups formed chemical bonds with the hydroxy groups on surface of tin oxide nanocrystals, clusters and/or related ions. This bond formation accelerated the nucleation and growth of tin oxide on the surface (Equations a–d).[43,44] The hydrophilic surface was, therefore, more effective for tin oxide deposition than the hydrophobic surface.

$$SnF_2 \xrightarrow{OH^-} SnF(OH) + F^- \xrightarrow{OH^-} Sn(OH)_2 + F^- \quad (a)$$

$$Sn(OH)_2 \longrightarrow SnO + H_2O \quad (b)$$

$$Sn(OH)_2 \longrightarrow SnO_2 + H_2 \quad (c)$$

$$SnO + H_2O \longrightarrow SnO_2 + H_2 \quad (d)^{[43,44]}$$

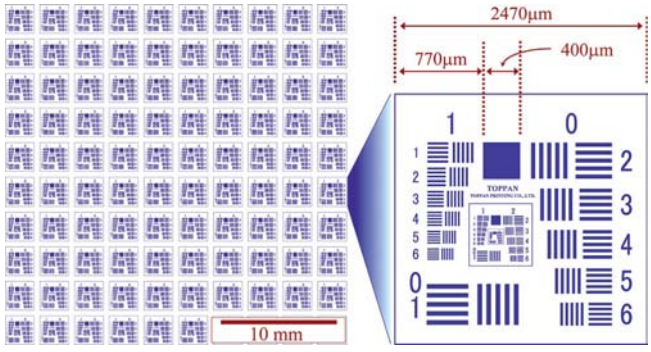

Figure 1. Design of a photomask for light irradiation.

Generation of gas was observed immediately after the addition of SnF_2 in water at 90 °C. The ion concentration, the valence of the ions, and the pH changed during the synthesis. They affected the formation of SnO and SnO_2. The nanocrystals adhered well to the irradiated surfaces and were not removed under running water or by an air spray. Direct crystallization of tin oxide on the films caused a high adhesive strength, which is required for sensors or solar cells. Some fluorine ions existed as dopants in tin oxide. Fluorine doping is known to enhance the performance of sensors and solar cells.[45] Residual fluorine ions remained in the solution.

Contact angle, wettability, and surface tension strongly relate to nucleation of tin oxide. The function $f(\theta)$ and the critical energy decrease from 1 to 0 as contact angle (θ) decreases (Supporting Information, Figure S1). Therefore, nucleation occurs more easily on a hydrophilic surface. This phenomenon can be explained by known mechanisms of crystal formation.

Additionally, the hydrophilic surface of ITO was covered with hydroxy groups. Their density was much higher than that of hydroxy groups on the hydrophobic surface of ITO before the irradiation. The initial ITO surface was covered with adsorbed organic molecules. They covered the pure surface of In_2O_3 crystals and increased the water contact angle. Hydroxy groups form chemical bonds with hydroxy groups on the surface of tin oxide nanocrystals, clusters, and/or related ions. The formation of these bonds accelerates the nucleation and growth of tin oxide on the surface. Therefore, the hydrophilic surface is more effective for tin oxide deposition than the hydrophobic surface.

Patterning of Tin Oxide on ITO/PET Films

The super-hydrophilic areas on the ITO/PET films were coated with tin oxide nanosheets in aqueous solution (Figure 2). On the other hand, the hydrophobic areas suppressed the deposition of tin oxide. Super-hydrophilic/hydrophobic surface modification enabled 2D patterning of tin oxide nanosheets on flexible ITO/PET films. The super-hydrophilic area was covered with the nanosheets uniformly (Figure 3a). They were of 100–300 nm in-plane size and 5–10 nm thickness (Figure 3b). Observation of the surface (Figure 3a,b) and the fractured cross section image (Figure 3c) reveals the morphology of the nanosheets clearly.

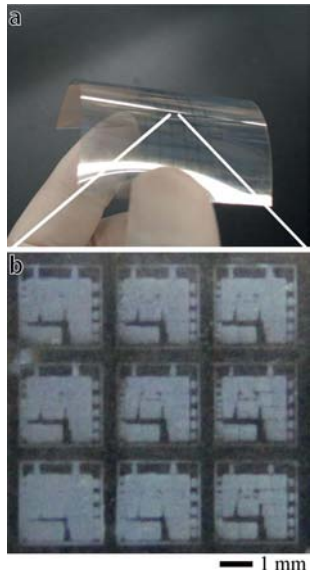

Figure 2. (a) Photograph of 2D patterns of tin oxide nanosheets on a flexible ITO/PET film. (b) Magnified area of (a) showing details of 2D patterns.

ITO/PET films with tin oxide nanosheets were characterized with XRD (Figure 4b). Their XRD pattern was similar to that of ITO/PET films without deposited tin oxide

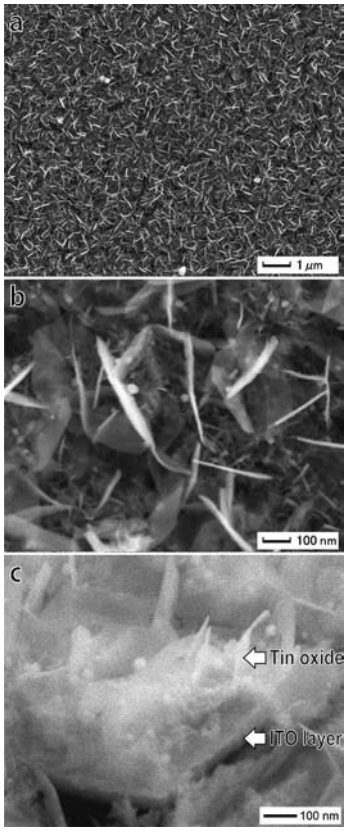

Figure 3. (a) FE-SEM image of tin oxide nanosheets on super-hydrophilic areas of the film. (b) Magnified area of (a) showing surface morphology of tin oxide nanosheets. (c) Tilted image of fracture cross-section of (b) showing sheet morphology of tin oxide nanosheets.

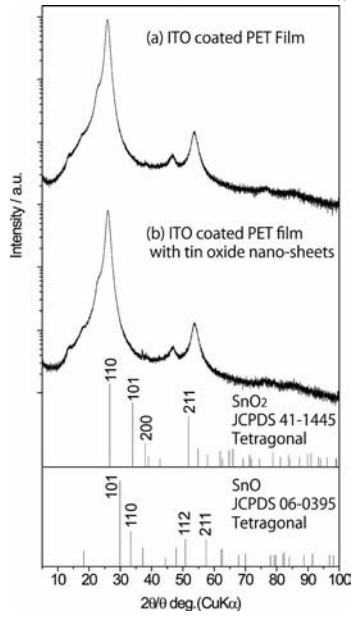

Figure 4. XRD patterns of (a) ITO-coated PET film, (b) ITO-coated PET film with tin oxide nanosheets, and JCPDS standard X-ray diffraction data for SnO_2 or SnO.

(Figure 4a). The tin oxide surface coating was very thin and did not give rise to intense X-ray diffraction peaks. The crystal phase of the surface coatings was evaluated with electron diffraction patterns obtained with TEM equipment modified as mentioned below.

The nanosheets were formed on ITO layers of PET films directly (Figure 4), as super-hydrophilic ITO surfaces accelerated the crystal growth of tin oxide. The surface of the ITO layer was covered with nanosheets of 5–10 nm size (Figure 4b). Some of them further grew to in-plane sizes of 100–300 nm (Figure 4b). Anisotropic growth of tin oxide crystals formed the sheet structure. Lattice fringes were observed from all areas of the sheets (Figure 5). Electron diffraction patterns revealed that the nanosheets in circles 1 and 2 were single crystals of SnO. Diffraction spots were clearly observed and assigned to SnO. Estimated lattice spacings matched those of SnO. Meanwhile, nanosheets in circle 3 (Figure 6) consisted of SnO and SnO_2. A small amount of SnO_2 crystallized at the initial stage of the immersion period.

The depth profile from XPS studies reveals the chemical composition of the nanosheets (Figure 7). The chemical composition of the topmost surface was estimated to be Sn/O = 1:1.87 (Table 1), which corresponds to SnO_2. The oxygen content would include a slight amount coming from surface contamination. The ratio changed to Sn/O = 1:0.75–0.93 (Table 1) during the sputtering. These values are similar to that of SnO. The ratio of oxygen to tin is known to decrease with sputtering. Electron diffraction patterns indicate that the structures are a mixture of SnO and SnO_2 as mentioned above. This affects the chemical composition.

In XPS analyses, indium and oxygen were observed from ITO layers after etching for 12 seconds. Carbon was detected from PET films after etching for 30 seconds. The nanosheets are composed of tin, oxygen, and fluorine, without contaminants (Figure 8a).

The spectral peak corresponding to Sn $3d_{5/2}$ was observed at 486.4 eV (Figure 8b). This value is similar to that of Sn^{4+} in SnO_2 (486.6 eV[46]) and higher than that of the Sn^{2+} site in SnO (485.9 eV[46]) or Sn metal (484.8 eV,[47] 484.85 eV,[48] 484.87 eV,[49] 484.9 eV,[50] 485.0 eV[51]). It suggests that tin atoms are positively charged by forming direct bonds with oxygen.

The O 1s peak at 530.4 eV (Figure 8c) corresponds to that of SnO. It indicates that oxygen atoms are negatively charged relative to neutral oxygen molecules (531.0 eV) possibly through the formation of direct bonds with tin atoms. The O1s peak is rather broad with a shoulder at high energies that confirms the presence of several contributions (Sn^{2+}–O, Sn^{4+}–O, –OH, C–O, etc.). This is consistent with the presence of a mixture of SnO and SnO_2.

The chemical composition of the topmost surface was estimated to be F/Sn = 0.082 (Table 1), including some fluorine from surface contamination, because SnF_2 was used as precursor and it was difficult to remove totally under running water. The F/Sn ratio decreased during the sputtering, and it reached a relatively constant value of F/Sn = 0.047–0.052. Fluorine remained even after the sputtering.

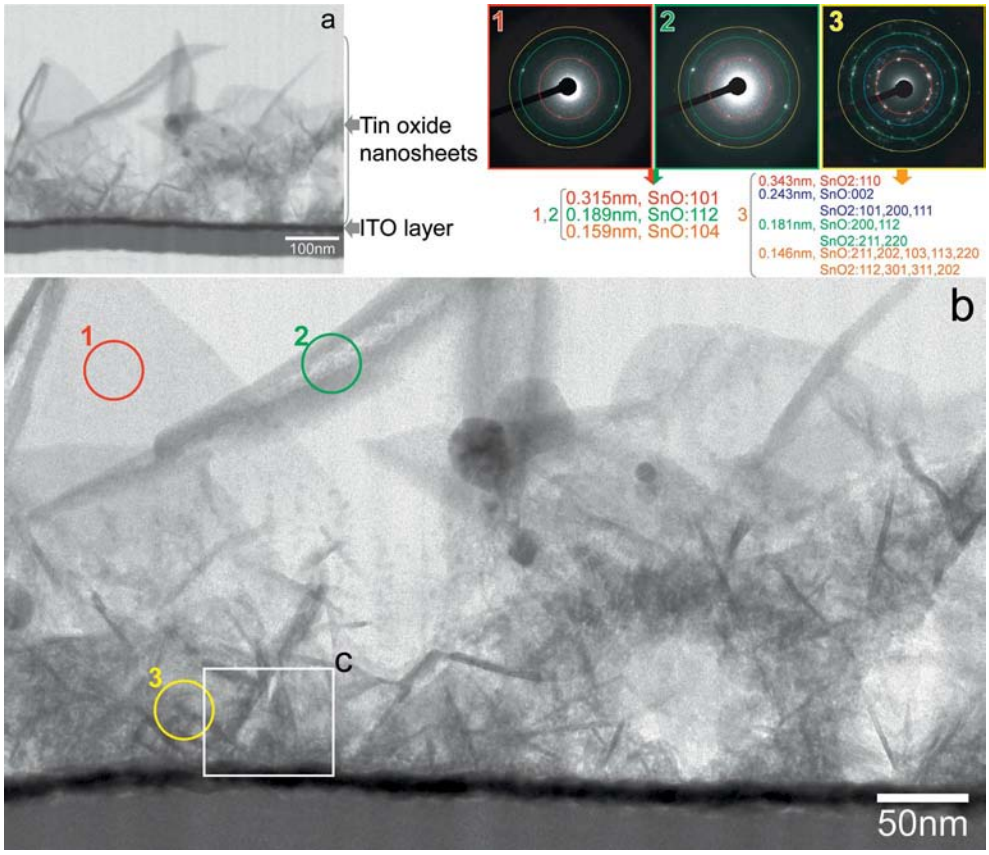

Figure 5. (a) Cross-section TEM images of tin oxide nanosheets on a flexible ITO/PET film. (b) Magnified area of (a) showing morphology of tin oxide nanosheets. (1–3) Electron diffraction patterns from circles in TEM image of (b).

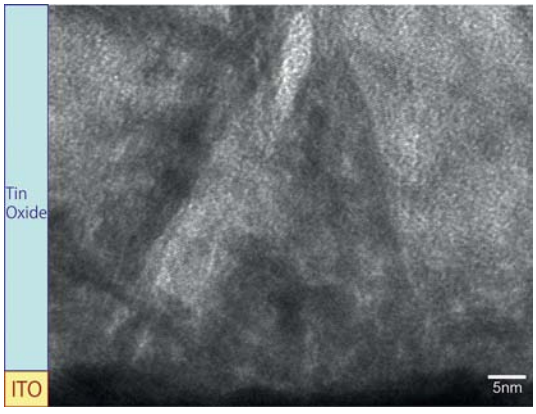

Figure 6. Magnified area of cross-section TEM image of tin oxide nanosheets on a flexible ITO/PET film showing the interface between tin oxide nanosheets and the ITO/PET film.

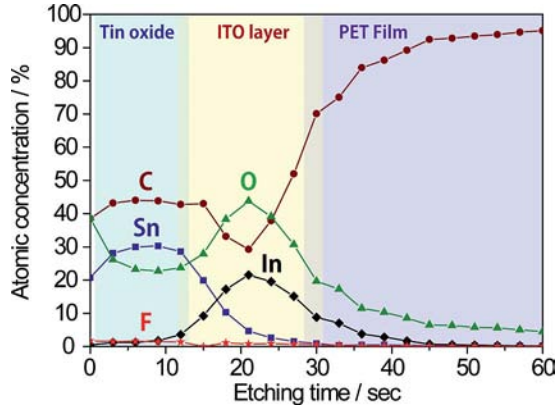

Figure 7. Atomic concentration depth profile of tin oxide nanosheets on a flexible ITO/PET film.

The F 1s peak was observed at 684.5 eV (Figure 8d). The binding energy is similar to that of fluorine atoms that exist as dopants in tin oxide (684.4 eV[52]), suggesting the presence of fluorine doping in the nanosheets. Fluorine doping in tin oxide is well known to be suitable for sensors and solar cells.[45] A key factor for these applications is the electronic conductivity, which increases with fluorine doping. The 2D patterns developed in this study can be applied in devices.

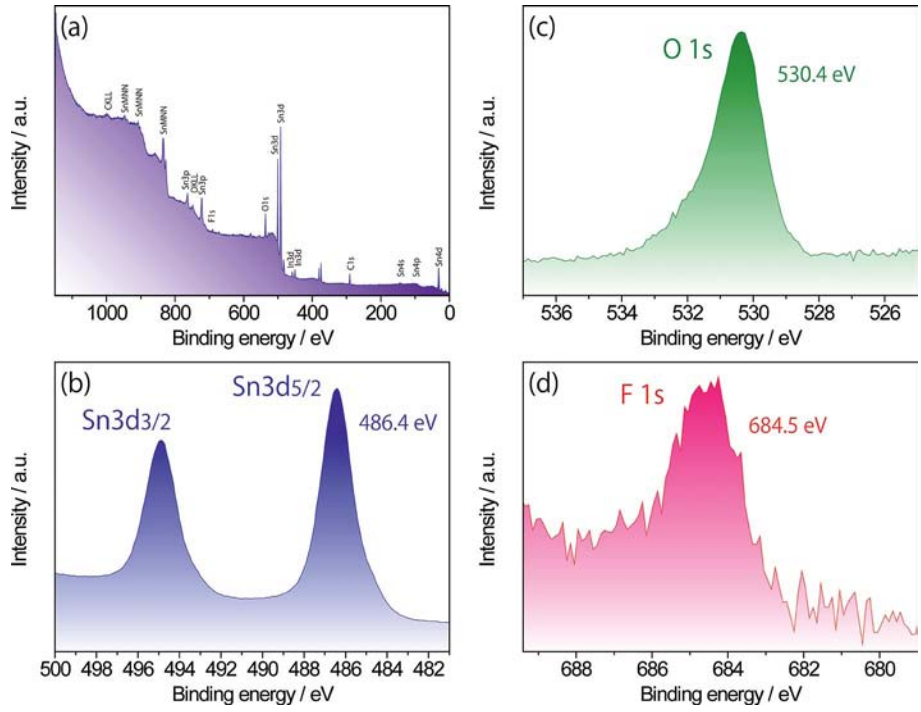

Figure 8. XPS spectra of tin oxide nanosheets on a flexible ITO/PET film. (a) Survey spectrum, (b) Sn 3d spectrum, (c) O 1s spectrum, and (d) F 1s spectrum.

Table 1. Atomic concentration and chemical ratio of tin oxide nanosheets on a flexible ITO/PET film.

Sn	20.70	28.08	29.99	30.25	28.54	(at%)
O	38.65	26.12	23.23	22.71	23.74	(at%)
F	1.69	1.45	1.53	1.42	1.35	(at%)
In	0.47	1.17	1.23	1.79	3.59	(at%)
F:Sn	0.082	0.052	0.051	0.047	0.047	
O:Sn	1.87	0.93	0.77	0.75	0.83	
Etching time	0	3	6	9	12	(sec)

For comparison, a high photocurrent was obtained from fluorine-doped tin oxide nanostructures on FTO substrates under light irradiation.[53] They were modified with dye-labeled protein or dye-labeled DNA. The high electronic conductivity of the structures contributed to the observation of a high photocurrent. Direct evaluation of the electronic conductivity of nanostructures is technically difficult, but it has intrinsic value and is now in progress.

Conclusions

A site-selective chemical reaction for tin oxide nanosheet formation was developed on flexible polymer films using super-hydrophilic surfaces. The films were exposed to light through a photomask to form hydrophobic and super-hydrophilic patterns. Chemical reaction proceeded in a site-selective manner only on super-hydrophilic areas in aqueous solutions containing SnF_2. The super-hydrophilic surface of ITO accelerated the chemical reaction, nucleation, and growth of tin oxide crystals, whereas the hydrophobic areas of the films suppressed formation of tin oxide structures. Tin oxide sheets grew to 100–300 nm in-plane size and 5–10 nm thickness. Consequently, 2D patterns of tin

oxide nanosheets were fabricated on flexible ITO/PET films. Site-selective chemical reaction will be applied to precise control of chemical reactions, surface coating, and two-dimensional patterning of various systems such as inorganic materials, organic materials, biomaterials, hybrid materials, and so on. This will open new avenues for flexible organic–inorganic hybrid devices.

Experimental Section

Poly(ethylene terephthalate) (PET) films were coated with transparent conductive indium tin oxide (ITO) layers. ITO layers of 120–160 nm thickness were coated on the films with the sputtering method. They had a sheet resistance of 10 Ω/square and a transparency of over 74%. They were exposed to vacuum ultraviolet light through a photomask for 10 min (VUV, low-pressure mercury lamp PL16–110, air flow, 100 V, 200 W, SEN Lights Co., 14 mW/cm^2 for 184.9 nm at a distance of 10 mm from the lamp, 18 mW/cm^2 for 253.7 nm at a distance of 10 mm the from lamp).

SnF_2 (Wako Pure Chemical Industries, Ltd., No. 202–05485, FW: 156.71, purity 90.0%) was used as received. Distilled water in polypropylene vessels (200 mL) were capped with polymer films and kept at 90 °C. SnF_2 (870.6 mg) was added and dissolved in the distilled water at 90 °C to a concentration of 5 mM.[54–57] The substrates were immersed in the middle of the solutions with the bottom up at an angle of 15° from perpendicular. The solutions were stored at 90 °C in a drying oven (Yamato Scientific Co., Ltd., DKN402) for 2 h without stirring. The substrates were rinsed under running water and dried with a strong air spray.

The surface morphology of ITO/PET films with tin oxide nanosheets were observed with a field emission scanning electron microscope (FE-SEM; JSM-6335FM, JEOL Ltd.). The crystal phase was evaluated with an X-ray diffractometer (XRD; RINT-2100V, Rigaku) with Cu-K_α radiation (40 kV, 30 mA). Diffraction patterns were evaluated by using data from the ICSD (Inorganic Crystal Structure Database) (FIZ Karlsruhe, Germany and NIST, USA) and FindIt. The ITO/PET films with tin oxide nanosheets were treated with a focused ion beam to evaluate cross-section images. Cross section images were observed with a transmission electron microscope (JEM2000FX, 200 kV, JEOL Ltd.). The crystal phase was evaluated with an electron diffraction unit built into the transmission electron microscope. The depth profile of the chemical composition was evaluated with an X-ray photoelectron spectroscopy (XPS, Kratos analytical, ESCA-3400, Shimadzu). The X-ray source (Mg-K_α, 1253.6 eV) was operated at 10 kV and 20 mA. The resolutions for survey analyses or narrow analyses, that is, the FWHM of $Ag3d_{5/2}$ spectrum, were 1.15 eV or 0.95 eV, respectively. Ag was selected for the evaluation of spectrum resolution and analysis conditions, because Ag is chemically stable and resistant to oxidation. It showed sharp $Ag3d_{5/2}$ peak without peaks of oxidized states. Step size (eV) or dwell time (sec) for survey analyses or narrow analyses were 1 eV, 150 s or 0.1 eV, 300 s, respectively. Spectra were corrected by using the standard binding energy of C–C bonds (C 1s, 284.6 eV) in surface contaminations. Surface contamination was almost removed during the first 3 seconds of etching.

Supporting Information (see footnote on the first page of this article): Model of a nucleated crystal on a substrate in a liquid.

Acknowledgments

The authors thank Dr. Shuji Sonezaki, Dr. Hitoshi Ohara, Dr. Makoto Bekki, Dr. Yoshimasa Yamanam, and Dr. Masako Ajimi of TOTO Ltd. Research Laboratory. This work was partially supported by Ministry of Economy, Trade and Industry (METI), Japan, as part of R&D for High Sensitivity Environment Sensor Components.

[1] J. Huang, N. Matsunaga, K. Shimanoe, N. Yamazoe, T. Kunitake, *Chem. Mater.* **2005**, *17*, 3513–3518.
[2] D. S. Ginley, C. Bright, *MRS Bull.* **2000**, *25*, 15–21.
[3] Y. Idota, T. Kubota, A. Matsufuji, Y. Maekawa, T. Miyasaka, *Science* **1997**, *276*, 1395–1397.
[4] H. Tokudome, Y. Yamada, S. Sonezaki, H. Ishikawa, M. Bekki, K. Kanehira, M. Miyauchi, *Appl. Phys. Lett.* **2005**, *87*, 213901–213903.
[5] T. M. Jyothi, S. Sugunan, B. S. Rao, *Green Chem.* **2000**, *2*, 269–271.
[6] R. S. Yuan, C. Lin, B. C. Wu, X. Z. Fu, *Eur. J. Inorg. Chem.* **2009**, 3537–3540.
[7] S. Mathur, S. Barth, *Small* **2007**, *3*, 2070–2075.
[8] S. Mathur, S. Barth, H. Shen, J. C. Pyun, U. Werner, *Small* **2005**, *1*, 713–717.
[9] Z. R. Dai, J. L. Gole, J. D. Stout, Z. L. Wang, *J. Phys. Chem. B* **2002**, *106*, 1274–1279.
[10] Y. Wang, J. Y. Lee, H. C. Zeng, *Chem. Mater.* **2005**, *17*, 3899–3903.
[11] Y. K. Liu, C. L. Zheng, W. Z. Wang, C. R. Yin, G. H. Wang, *Adv. Mater.* **2001**, *13*, 1883–1887.
[12] J. Q. Sun, J. S. Wang, X. C. Wu, G. S. Zhang, J. Y. Wei, S. Q. Zhang, H. Li, D. R. Chen, *Cryst. Growth Des.* **2006**, *6*, 1584–1587.
[13] R. S. Yang, Z. L. Wang, *J. Am. Chem. Soc.* **2006**, *128*, 1466–1467.
[14] J. H. Duan, S. G. Yang, H. W. Liu, J. F. Gong, H. B. Huang, X. N. Zhao, R. Zhang, Y. W. Du, *J. Am. Chem. Soc.* **2005**, *127*, 6180–6181.
[15] H. Ohgi, T. Maeda, E. Hosono, S. Fujihara, H. Imai, *Cryst. Growth Des.* **2005**, *5*, 1079–1083.
[16] H. Uchiyama, H. Imai, *Cryst. Growth Des.* **2007**, *7*, 841–843.
[17] Y. L. Zhang, Y. Liu, M. L. Liu, *Chem. Mater.* **2006**, *18*, 4643–4646.
[18] L. Ding, C. Q. Li, W. W. Zhou, H. B. Chu, X. A. Sun, Z. Cao, Z. H. Yang, C. H. Yan, Y. Li, *Eur. J. Inorg. Chem.* **2010**, 4357–4362.
[19] X. C. Wu, L. F. Chi, H. Fuchs, *Eur. J. Inorg. Chem.* **2005**, 3729–3733.
[20] N. Shirahata, W. Shin, N. Murayama, A. Hozumi, Y. Yokogawa, T. Kameyama, Y. Masuda, K. Koumoto, *Adv. Funct. Mater.* **2004**, *14*, 580–588.
[21] Y. Masuda, M. Kondo, K. Koumoto, *Cryst. Growth Des.* **2009**, *9*, 555–561.
[22] Y. Masuda, M. Yamagishi, K. Koumoto, *Chem. Mater.* **2007**, *19*, 1002–1008.
[23] Y. Masuda, *J. Ceram. Soc. Jpn.* **2007**, *115*, 101–109.
[24] Y. Masuda, N. Kinoshita, F. Sato, K. Koumoto, *Cryst. Growth Des.* **2006**, *6*, 75–78.
[25] T. Nakanishi, Y. Masuda, K. Koumoto, *Chem. Mater.* **2004**, *16*, 3484–3488.
[26] E. S. Shibu, B. Radha, P. K. Verma, P. Bhyrappa, G. U. Kulkarni, S. K. Pal, T. Pradeep, *Acs Appl. Mater. Interfaces* **2009**, *1*, 2199–2210.
[27] D. F. Acevedo, H. J. Salavagione, A. F. Lasagni, E. Morallon, F. Mucklich, C. Barbero, *Acs Appl. Mater. Interfaces* **2009**, *1*, 549–551.
[28] H. Mizuno, J. M. Buriak, *Acs Appl. Mater. Interfaces* **2009**, *1*, 2711–2720.
[29] B. Li, R. Franking, E. C. Landis, H. Kim, R. J. Hamers, *Acs Appl. Mater. Interfaces* **2009**, *1*, 1013–1022.
[30] M. Geissler, E. Roy, G. A. Diaz-Quijada, J. C. Galas, T. Veres, *Acs Appl. Mater. Interfaces* **2009**, *1*, 1387–1395.
[31] Y. Masuda, K. Kato, *Chem. Mater.* **2008**, *20*, 1057–1063.

[32] Z. Tebby, O. Babot, T. Toupance, D. H. Park, G. Campet, M. H. Delville, *Chem. Mater.* **2008**, *20*, 7260–7267.
[33] D. Gutierrez-Tauste, I. Zumeta, E. Vigil, M. A. Hernandez-Fenollosa, X. Domenech, J. A. Ayllon, *J. Photochem. Photobiol. A: Chem.* **2005**, *175*, 165–171.
[34] T. Yamaguchi, N. Tobe, D. Matsumoto, H. Arakawa, *Chem. Commun.* **2007**, 4767–4769.
[35] Y. Masuda, T. Sugiyama, W. S. Seo, K. Koumoto, *Chem. Mater.* **2003**, *15*, 2469–2476.
[36] Y. Masuda, S. Ieda, K. Koumoto, *Langmuir* **2003**, *19*, 4415–4419.
[37] Y. Masuda, N. Saito, R. Hoffmann, M. R. De Guire, K. Koumoto, *Sci. Technol. Adv. Mater.* **2003**, *4*, 461–467.
[38] Y. Masuda, Y. Jinbo, T. Yonezawa, K. Koumoto, *Chem. Mater.* **2002**, *14*, 1236–1241.
[39] Y. Masuda, T. Sugiyama, H. Lin, W. S. Seo, K. Koumoto, *Thin Solid Films* **2001**, *382*, 153–157.
[40] Y. Masuda, Y. F. Gao, P. X. Zhu, N. Shirahata, N. Saito, K. Koumoto, *J. Ceram. Soc. Jpn.* **2004**, *112*, 1495–1505.
[41] J. H. Xiang, Y. Masuda, K. Koumoto, *Adv. Mater.* **2004**, *16*, 1461–1464.
[42] S. Sawada, Y. Masuda, P. X. Zhu, K. Koumoto, *Langmuir* **2006**, *22*, 332–337.
[43] C. F. Baes, R. E. Mesiner, *The Hydrolysis of Cations*, John Wiley & Sons, Inc., Wiley-Interscience, New York, **1976**.
[44] C. Ararat Ibarguena, A. Mosqueraa, R. Parrab, M. S. Castrob, J. E. Rodríguez-Páeza, *Mater. Chem. Phys.* **2007**, *101*, 433–440.
[45] C. H. Han, S. D. Han, I. Singh, T. Toupance, *Sensors Actuators B-Chem.* **2005**, *109*, 264–269.
[46] M. Kwoka, L. Ottaviano, M. Passacantando, S. Santucci, G. Czempik, J. Szuber, *Thin Solid Films* **2005**, *490*, 36–42.
[47] A. C. Parry-Jones, P. Weightman, P. T. Andrews, *J. Phys. C Sol. State Phys.* **1979**, *12*, 1587–1600.
[48] C. D. Wagner, W. M. Riggs, L. E. Davis, J. F. Moulder, G. E. Muilenberg, *Handbook of X-ray Photoelectron Spectroscopy*, Perkin–Elmer Corp., Physical Electronics Div., Eden Prairie, Minnesota, **1979**.
[49] M. Pessa, A. Vuoristo, M. Vulli, S. Aksela, J. Väyrynen, T. Rantala, H. Aksela, *Phys. Rev. B* **1979**, *20*, 3115–3123.
[50] A. W. C. Lin, N. R. Armstrong, T. Kuwana, *Anal. Chem.* **1977**, *49*, 1228–1235.
[51] C. D. Wagner, *Discuss. Faraday Soc.* **1975**, *60*, 291–318.
[52] A. I. Martinez, L. Huerta, J. de Leon, D. Acosta, O. Malik, M. Aguilar, *J. Phys. D Appl. Phys.* **2006**, *39*, 5091–5096.
[53] Y. Masuda, T. Ohji, K. Kato, M. Ajimi, M. Bekki, S. Sonezaki, *J. Am. Ceram. Soc.*, submitted.
[54] Y. Masuda, K. Kato, *J. Cryst. Growth* **2009**, *311*, 593–596.
[55] Y. Masuda, K. Kato, *Polym. Adv. Technol.* **2010**, *21*, 211–215.
[56] Y. Masuda, T. Ohji, K. Kato, *J. Am. Ceram. Soc.* **2010**, *93*, 2140–2143.
[57] Y. Masuda, T. Ohji, K. Kato, *Thin Solid Films* **2009**, *518*, 850–852.

Received: January 21, 2011
Published Online: May 12, 2011

